Optical properties of nanocrystalline WO_3 and WO_{3-x} thin films prepared by DC magnetron sputtering

Malin B Johansson[1,*], Burkhard Zietz[2], Gunnar A Niklasson[1] and Lars Österlund[1,*]

[1]Division of Solid State Physics, Department of Engineering Sciences, The Ångström Laboratory, Uppsala University, P.O. Box 534, SE-75121 Uppsala, Sweden.

[2]Division of Physical Chemistry, Department of Chemistry, The Ångström Laboratory, Uppsala University, P.O. Box 523, SE-75120 Uppsala, Sweden.

Contact authors: M. B. Johansson:majo4400@gmail.com, lars.osterlund@angstrom.uu.se

Abstract

The optical properties of tungsten trioxide thin films prepared by DC magnetron sputtering, with different oxygen vacancy (V_o) concentration, have been studied by spectrophotometry and photoluminescence (PL) emission spectroscopy. Absorption and PL spectra show that the films exhibit similar band gap energies, $E_g \approx 2.9$ eV. The absorption spectra of the films show two pronounced absorption bands in the near-infrared region. One peak (P1) is located at approximately 0.7 eV, independent of V_o concentration. A second peak (P2) shifts from 0.96 eV to 1.16 eV with decreasing V_o concentration. Peak P1 is assigned to polaron absorption due to transitions between tungsten sites ($W^{5+} \rightarrow W^{6+}$), or an optical transition from a neutral vacancy state to the conduction band, $V_o^{0} \rightarrow W^{6+}$. The origin of peak P2 is more uncertain, but may involve +1 and +2 charged vacancy sites. The PL spectra show several emission bands in the range 2.07 to 3.10 eV in the more sub-stoichiometric, and 2.40 to 3.02 eV in the less sub-stoichiometric films. The low energy emission bands agree well with calculated optical transition energies of oxygen vacancy sites, with dominant contribution from neutral and singly charged vacancies in the less sub-stoichiometric films, and additional contributions from doubly charged vacancy sites in the more sub-stoichiometric films.

I. INTRODUCTION

Tungsten trioxide (WO_3) is an interesting material, which shows promising properties for applications in several important sustainable technologies, such as smart windows, gas sensors, and as a photo-catalyst for air cleaning and water splitting.[1, 2] WO_3 is, however, easily reducible. Sub-stoichiometry alters the physical properties of tungsten oxides, and yields compounds with e.g. different color and electrical conductivity. In addition, several phases of WO_3 exist in a close range around room temperature and atmospheric pressure,[3, 4] each with slightly different structure and electronic properties. It is therefore important to systematically characterize WO_3 materials with known phase composition, and compare them with similar sub-stoichiometric WO_{3-x} compounds.

In sub-stoichiometric WO_{3-x}, it has been reported that localized states are located close to an oxygen vacancy, or a specific W atom.[1] In an optical transition, an electron is transferred from one localized state to a neighboring one. The optical transitions can be described with different models. One description is in terms of an intervalence transfer between two adjacent localized states.[5] In the case of tungsten oxide, the states involved would be localized on W sites.[6] In the sub-stoichiometric case also transitions between oxygen vacancy states and W sites must be taken into account. A very strong electron-phonon interaction can in itself lead to localization of an electron from the conduction band,[7, 8] and the intervalence transfer model then becomes equivalent to polaron absorption models.[7-10] In both cases, an electron in the localized state can in a first approximation be described as being trapped at the bottom of a parabolic potential well. The potential wells of adjacent localized states are taken to be overlapping. The energy difference of the ground states of the parabolas to the point where they intersect, is the activation energy for electron transport.[5, 8] The optical transition is "vertical" from the ground state of one parabola to a higher energy in the second parabolic well, requiring photon energies four times the activation energy.[5, 8] Polaron theory was first applied to WO_3 by Salje[11] and Schirmer et al.[12] The polaron binding energy in WO_3 has been computed from experimentally accessible quantities,[13] as well as theoretically,[14] and the polaron ground state was found to be located 0.15-0.2 eV below the conduction band minimum (CBM), giving an optical absorption energy of 0.6-0.8 eV.[13] A different model, applicable to sub-stoichiometric WO_{3-x}, is to view the optical absorption and photoluminescence transitions as due to electronic transitions at oxygen vacancy sites. These vacancies can be neutral (V_o^0), singly charged (V_o^{1+}) or doubly charged (V_o^{2+}). In a recent theoretical study,[15] it was shown that hybrid density functional calculations are a versatile tool for studying the electronic states in WO_3. Furthermore, Gallino et al. devised a method to calculate the positions of optical and thermal transition energy levels.[16] Wang et al. [17]applied this method to WO_{3-x} employing two different hybrid functionals, which both gave reasonable values of the band gap energy. It was shown that both the thermal ionization levels (allowing lattice relaxation) and the optical transition

state energy levels describing transitions between the different charge states are located in the band gap. This is in contrast to the Deb O vacancy model,[18] where the defect levels are expected to be in the valence band if they hold two electrons (V_o^{0}), in the band gap when one electron is left at the vacancy (V_o^{1+}), or in the conduction band when two electrons are removed from the vacancy (V_o^{2+}).

In this study we have experimentally investigated monoclinic, nanocrystalline tungsten oxide thin films prepared with DC magnetron sputtering with optical spectroscopy to characterize the influence of oxygen vacancies on their optical properties. Optical absorption and photoluminescence (PL) spectroscopy are useful techniques to obtain information on localized states in the band gap. Hitherto, comparatively few PL studies have been reported on WO_3.[19-22] PL emission can be associated with decay of an electron from the conduction band (CB) directly back to the valence band (VB), into a charged vacancy state (V_o^{1+} or V_o^{2+}), or from the vacancy state (V_o^{0} or V_o^{1+}) to the VB. An electron can also decay non-radiatively to a localized state and then further decay by a PL process to the VB. The transitions can occur from a thermally equilibrated state at the bottom of a potential well to a non-relaxed state, or vice versa. Here we relate experimental data with possible optical and PL transitions in nanocrystalline WO_3.

II. MATERIALS AND METHODS

A. Thin film fabrication

Tungsten oxide (WO_3) thin films were prepared by reactive DC magnetron sputtering using a versatile deposition system based on a Balzers UTT 400 unit. The films were sputtered on CaF_2 substrates (Crystran Ltd., Pole, UK.). More information about the experimental details can be found elsewhere.[23, 24] The O_2 /Ar ratio was kept at 0.43, and the samples were sputtered at a substrate temperature of T_s = 553 K, and post-annealed at T_a = 673 K for 1 h in air. Samples were sputtered at working pressures, P_{tot} = 10, 15, 20, 25 and 30 mTorr. The deposition rate varied as a function of P_{tot} from 36 nm min^{-1} at P_{tot} = 10 mTorr to 11 nm min^{-1} at P_{tot} = 30 mTorr. WO_3 thin films sputtered on CaF_2 substrates were highly transparent. Films prepared at P_{tot} = 10 mTorr exhibited a slightly bluish color, indicating sub-stoichiometry. The samples sputtered at P_{tot} = 30 mTorr were slightly yellowish and red, characteristic of stoichiometric WO_3. In previous studies we have reported on the physical properties of tungsten oxide films prepared in this manner.[23-25] From cyclic voltammetry (CV), a lower limit of the concentration of trap states in the band gap was calculated.[25] These trap states were associated with oxygen vacancies in the thin film, and the measured concentrations correlated well with previous approximate values obtained from near infrared (NIR) absorption.[24] An oxygen vacancy concentration of $x \approx 0.005$ (determined by an average over three films) was inferred in the more sub-stoichiometric WO_{3-x} films, prepared at P_{tot} = 10 mTorr, while the less sub-stoichiometric films prepared at P_{tot} = 30

mTorr showed vacancy concentrations of $x \approx 0.001$ (determined by an average over four films).[25] It was shown that the films mainly exhibited the monoclinic γ-WO_3 phase with a fraction of the monoclinic ε-phase and a slight strain in films primarily at P_{tot} = 10 mTorr.[24]

B. Spectrophotometry

The optical properties of the WO_3 films were measured with a Perkin-Elmer Lambda 900 double-beam UV/Vis/NIR spectrophotometer equipped with an integrating sphere and a Spectralon reflectance standard. The absorption coefficient α as a function of wavelength λ was determined by spectrophotometry from the special absorption:[26]

$$\alpha(\lambda) = \frac{1}{d} \ln\left(\frac{1 - R(\lambda)}{T(\lambda)}\right), \tag{1}$$

where d is the thickness of the film.

The film thicknesses of the fabricated WO_3 films were uniform, and gave rise to interference fringes in the optical spectra. The basic equation for interference fringes is

$$2nd = m\lambda, \tag{2}$$

where m is an integer for maxima and a half integer for minima. Eqn. 2 contains the product of n and d, and cannot be used to extract independent values for n or d. However, by using the method introduced by Swanepoel for a weak to medium absorbing film, d and n can be decoupled using the interference fringes in the transmittance spectra by the formula:[27]

$$n = \left[N + \left(N^2 - n_s^{\,2}\right)^{1/2}\right]^{1/2}, \tag{3}$$

where

$$N = 2n_s \frac{T_M - T_m}{T_M T_m} + \frac{n_s^2 + 1}{2} \tag{4}$$

Here n_s is the refractive index for the substrate (CaF_2 in our case), T_M and T_m are the transmittance at the extremes of the transmittance fringes, considered as continuous functions of λ in the analysis (M = maximum; m = minimum). From eqn. 3 n can be calculated. Once n is known, d can be calculated by means of eqn. 2 using n at two adjacent maxima as follows:

$$d = \frac{\lambda_1 \lambda_2}{2\left(\lambda_1 n_2 - \lambda_2 n_1\right)}, \tag{5}$$

where the subscript numbers denote two adjacent maxima.

In the near-infrared range T and R were fitted to an optical oscillator model using the Scout software, in order to extract optical constants.[28] The long-wavelength dielectric constant $\varepsilon_0 \sim 3.6$ was obtained by iterative fitting using previously published data as the starting value.[23]

Gaussian functions were employed to fit the imaginary part of the dielectric function $\varepsilon_2(\lambda)$ in the near-infrared region in order to extract peak position, width and amplitude, according to,

$$\varepsilon_2\left(\lambda\right) = \sum_{i=1}^{2} a_i e^{\left(\frac{(2\pi c/\lambda) - b_i}{2w_i}\right)^2}, \tag{6}$$

where a is the amplitude, b the position of the center of the peak, and w the width of the peak. The program computed the real part of the dielectric function $\varepsilon_1(\lambda)$ by a Kramer-Kronig relation. The dielectric function was obtained by iterative fitting to experimental data.

C. Photoluminescence

Photoluminescence emission measurements were performed using a Horiba Jobin Yvon Fluorolog instrument (Model FL3-222). The signal was automatically corrected for wavelength dependent instrument sensitivity, and normalized with a reference signal to compensate for lamp fluctuations. The measurements were performed in backscattering geometry employing 30° angle of incidence of

the excitation beam with respect to the surface normal, and the detection optics aligned along the surface normal. A monochromator slit width resulting in a spectral resolution of 5 nm was used.

The interference fringes due to multiple reflections at the WO_3 film interfaces, which are seen in the optical transmission spectra, were also seen in the PL spectra. They must be corrected for to extract the intrinsic luminescence peaks. We distinguish between the luminescent intensity emerging from a plane *z* inside the WO_3 film, and going directly towards the detector through the air/WO_3 interface (denoted $I_{a/w}$), and the intensity, which is reflected back at the WO_3/CaF_2 interface ($I_{w/c}$), and then directed onto the detector through the air/WO_3 interface.[29] In the former case we have:

$$I_{a/w}(z) = A_{a/w}(z) A^*_{a/w}(z), \tag{7}$$

where $A_{a/w}(z)$ is the complex amplitude of the wave

$$A(z)_{a/w} = \frac{t_{a/w} \exp\left(-j\frac{2\pi n(\lambda)}{\lambda} z\right) \exp\left(-\frac{\alpha(\lambda)}{2} z\right)}{1 - r_{w/c} r_{a/w} \exp\left(-j\frac{2\pi n(\lambda)}{\lambda} 2d\right) \exp\left(-\alpha(\lambda) d\right)}, \tag{8}$$

where $r_{a/w}$, $t_{a/w}$, $r_{w/c}$ and $t_{w/c}$ are the Fresnel coefficients for reflection and transmission at the air/WO_3 and WO_3/CaF_2 interfaces, respectively. The refractive index for WO_3 was calculated in the wavelength range 350-700 nm using the Swanepoel method presented above. This refractive index was then used to calculate the Fresnel coefficients at each wavelength.

The luminescence intensity $I_{w/c}$ from the plane *z*, which is reflected back from the CaF_2 interface, and then emerges from the WO_3/air interface, is expressed as

$$I_{w/c}(z) = A_{w/c}(z) A^*_{w/c}(z), \tag{9}$$

where

$$A_{w/c}(z)=\frac{t_{a/w}r_{w/c}\exp\left(-j\frac{2\pi n(\lambda)}{\lambda}(2d-z)\right)\exp\left(-\left(\frac{\alpha(\lambda)}{2}\right)(2d-z)\right)}{1-r_{w/c}r_{a/w}\exp\left(-j\left(\frac{2\pi n(\lambda)}{\lambda}\right)2d\right)\exp(-\alpha(\lambda)d)}. \quad (10)$$

Neglecting diffusion of photo-excited electrons in the film, their distribution is proportional to $\alpha_{ex}\ exp(-\alpha_{ex}z)$ where $\alpha_{ex} = \alpha_{ex}(\lambda_{ex})$ is the absorption coefficient in the thin film at the excitation wavelength, λ_{ex}. The absorption corrected intensity at the detector for backward and forward propagating light from depth z in the film then becomes

$$I_{(a/w)',(w/c)'}(z)=I_{a/w,w/c}(z)\alpha_{ex}\exp(-\alpha_{ex}z) \quad (11)$$

Integration over z leads to the an interference function, IF, which includes multiple reflections transmission and absorption of the luminescence coming from the whole film, viz:[29]

$$IF=\int_0^d\left(I_{w/c'}(z)+I_{a/w'}(z)\right)dz \quad (12)$$

The IF is proportional to the total intensity of luminescence from the whole film. The PL spectra reported in this study were corrected for interference effects by dividing the measured spectra with the IF function (eqn. 12).

III. RESULT AND DISCUSSION

A. Spectrophotometry

Figure 1 shows the absorption coefficient for WO_3 films prepared at P_{tot} = 10 and 30 mTorr. The optical interband absorption is evident at wavelengths below about 440 nm. In the NIR range a broad absorption peak is observed, which is much stronger in the more sub-stoichiometric film prepared at P_{tot} = 10 mTorr. The absorption in the NIR region has previously been observed in sub-stoichiometric WO_{3-x}, attributed to polaron absorption, and interpreted in terms of polaron theory.[11, 13, 30] Figure 1b

shows a semi-logarithmic plot of α vs. wavelength close to the band edge. The small oscillations at $\lambda >$ 440 nm are due to interference effects not completely corrected for by eqn. (1). Underlying these oscillations, a wavelength dependence resembling an Urbach tail[31, 32] is seen in the region between 440 and 480 nm. At 440 nm (2.82 eV) the slope of the curve changes and this is marked by a solid line in Fig. 1b. This denotes the demarcation energy, which has been used to separate the Urbach tail from optical interband excitation.[31]

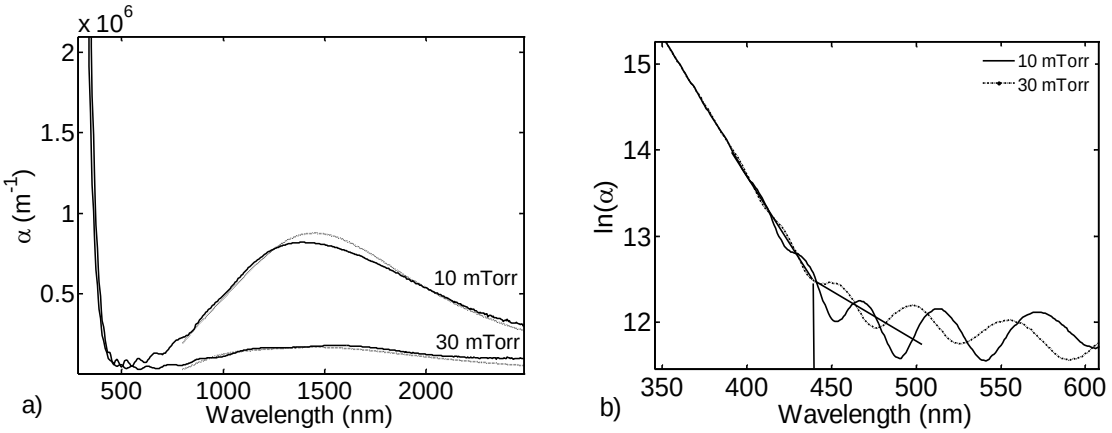

Figure 1 The absorption coefficient α for films prepared at P_{tot} = 10 and 30 mTorr, d = 1017 and 857 nm, respectively; a) α from eqn. 1 (solid line) in the wavelength range 350-2500 nm and fitted curves in the wavelength range 800-2500 nm (dotted lines) for the 10 and 30 mTorr samples. b) The natural logarithm of α in the wavelength range 350 - 600 nm. The straight line between 440 and 500 nm denotes an average of the interference fringes and approximates the "interference-free" absorption.

The absorption in the NIR range was fitted by the simulation program Scout[28] in which the imaginary part of the dielectric function ε_2 was approximated with two Gaussian functions (Figure 2a). It is evident that the NIR absorption can be accurately described by two peaks, here called P1 and P2, which have different relative strength depending on P_{tot}. In Figure 2b the energy and amplitude of the two ε_2 peaks are shown as a function of P_{tot}. The P1 peak shows the highest amplitude with a maximum at P_{tot} = 10 mTorr, and then decreases with increasing P_{tot}. The peak position of P1 stays constant at ~ 0.73 eV. The energy position of the P2 peak varies from 0.96 to 1.16 eV with increasing P_{tot}. The P2 absorption peak has lower amplitude compared to P1, and appears as a shoulder on the P1 peak, which is difficult to discern at low P_{tot}.

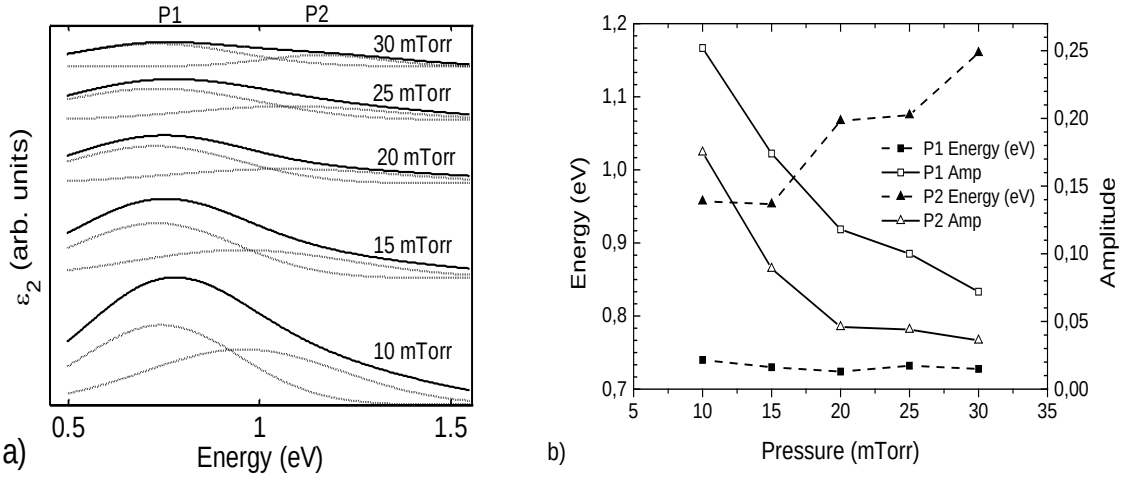

Figure 2 a) Best fits of ε_2 in the NIR region between 0.5 – 1.55 eV (0.80 – 2.47 μm) for WO_3 films prepared at different P_{tot} between 10 and 30 mTorr with the deconvoluted peaks P1 and P2 shown as dashed lines, b) Energy and amplitude of the P1 and P2 ε_2 peaks as a function of P_{tot}.

There are two basic frameworks for the interpretation of the optical absorption spectra. The first is polaron theory.[13] In this process electrons are excited from W^{5+} states to conduction band W^{6+} states, and the electron-phonon interaction leads to self-trapping in a localized state below the CBM. Alternatively, the optical transitions may be attributed to internal electronic transitions at the oxygen vacancy sites (V_o).[33] Recent hybrid functional DFT calculations of sub-stoichiometric γ-WO_3 have shown that O vacancy induced states below the Fermi level in γ-WO_{3-x} are strongly dependent on crystal direction and O vacancy concentration,[17] in qualitative agreement with the DFT calculation by Chatten et al.[34] At low defect concentrations (x = 0.06) Wang et al. showed that the vacancy induced states were located in the band gap about 0.5 – 1.0 eV below the conduction band minimum,[17] depending on choice of hybrid functional. In what follows we will compare with computations using the B3LYP functional[17], since the direct band gap value for this case is closer to the previously measured one for our WO_3 films.[23]

The position of peak P1 is close to the predicted energy of an optical transition between "intermediate" polaronic states in WO_3, with polaron radius ≈ 6 Å.[13] In this picture the polaron binding energy is inferred to be 0.18 eV below the CBM. However, the analogous optical transition of an electron from a neutral O vacancy to the CBM (which is mainly W5d character), $V_o^0 \rightarrow W^{6+}$, was predicted to have very similar excitation energy (0.73 eV) using computations with the B3LYP functional.[17] Peak P1 stays at the same energy irrespective of P_{tot} but its strength increases with increasing O vacancy concentration (decreasing P_{tot}). We note that the number of W^{5+} states must be equal to the number of V_0^{1+} vacancies because of charge conservation. Hence it may not be possible to distinguish polaronic

$W^{5+} \rightarrow W^{6+}$ transitions from ($V_o^{0} \rightarrow W^{6+}$) ones based on the optical spectra alone, since they are predicted to occur at very similar energies. Furthermore, both types of transitions are expected to be more prominent when the concentration of oxygen vacancies is higher, which is realized at lower P_{tot}.

The interpretation of peak P2 is more uncertain. The different behaviors of P1 and P2 as a function of deposition pressure (i.e. O vacancy concentration) suggest that they should be assigned to different mechanisms. Schirmer and Salje[35] have in a series of papers, employing electron spin resonance measurements, reported on the formation of "intermediate" polarons, with extension far beyond nearest neighbor lattice sites, and bipolarons,[36] i.e. diamagnetic paring of electrons at neighboring lattice sites, in the low-temperature ε- phase of very pure crystalline WO_3. The "intermediate" polaron is precisely the $W^{5+} \rightarrow W^{6+}$ transition discussed above; in the ε-phase it was shown to exhibit optical absorption at 0.71 eV. Interestingly, bipolaron absorption was inferred at ≈ 1 eV. The existence of bipolarons in an oxygen deficient ε- phase WO_3 is also supported by density functional theory calculations.[34] Polaron absorption in the ε- phase is relevant to this work, since we have previously shown that the more sub-stoichiometric WO_{3-x} thin films contain a minor contribution of the ε-phase.[23, 24] Intermediate polaron absorption in the ε-phase may contribute to the P1 peak in Fig. 2, in particular at low P_{tot} . The decreasing amplitude of P2 as a function of P_{tot} in Fig. 2 may then be an indication of a decreasing fraction of ε-phase with increasing P_{tot}, in accordance with experiments.[18] A possible explanation of the peak shift of P2 is, however, difficult to rationalize in this picture, which suggests that other optical transitions are contributing strongly to P2.

Alternatively, the P2 peak may be attributed to internal electronic transitions confined at the oxygen vacancy sites (V_o).[33] To compare with optical absorption data we have to consider the optical transition energies. We may then speculate that the P2 peak is due to different transitions between charged O vacancy levels; the most probable being $V_o^{0} \rightarrow V_o^{2+}$ and $V_o^{1+} \rightarrow V_o^{2+}$ transitions, which are predicted to occur at energies of 0.86 eV and 0.99 eV, respectively.[17] The P_{tot} dependence of the P2 peak position can in this model be explained by different concentrations of O vacancies, which change the relative contributions of the different optical transitions. The energy dependence would in this picture arise from different distribution of V_o^{0}, V_o^{1+}, and V_o^{2+} states with increasing sub-stoichiometry.

B. Photoluminescence

Figure 3 shows the photoluminescence (PL) and transmission (T) spectra for a WO_3 film prepared at P_{tot} = 30 mTorr, corresponding to a close to stoichiometric WO_3 film. It is evident that the interference fringes due to multiple reflections at the interfaces in the thin WO_3 film are present in both spectra. It is important to correct for these interference fringes in order to interpret the PL spectra correctly.

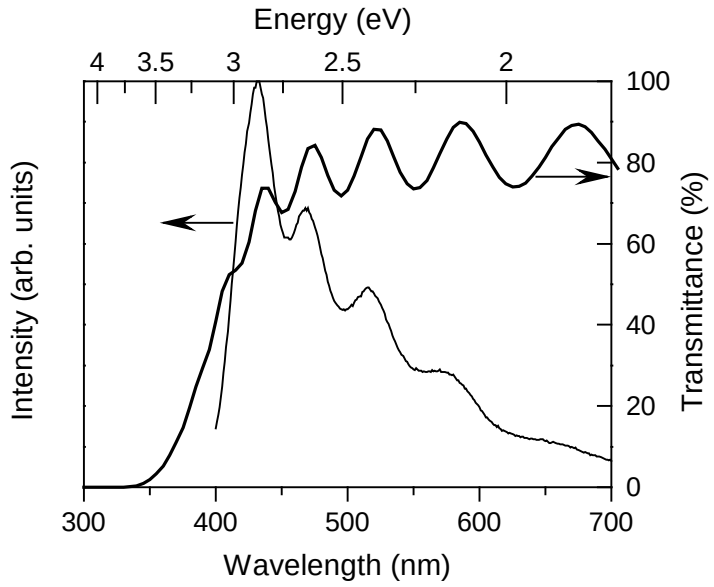

Figure 3 Transmittance (T) and normalized photoluminescence (PL) emission spectra of a WO_3 film sputtered at P_{tot} = 30 mTorr employing an excitation wavelength λ_{ex} = 380 nm.

By using the interference (IF) function based on Fresnel's equations described in section II.B the contribution from the interference fringes can be taken into account. The validity of the model is shown in Fig. 4 (a) and (b) where the IF function is plotted together with measured PL emission at an excitation wavelength λ_{ex} = 380 nm. The ratio of these two curves is shown as the curve labeled PL/IF. It is apparent that the peaks originating from interference are eliminated in the PL/IF curves. Figure 5 shows the IF corrected PL emission spectra of WO_3 films prepared at (a) P_{tot} = 30 mTorr, and (b) 10 mTorr, respectively, at different excitation energies: λ_{ex} = 350, 380, 400 and 420 nm, respectively. A summary of the peak energies and their relative peak intensity is shown in Table 1. The films sputtered at P_{tot} = 10 mTorr exhibit 6 emission peaks, whereas the films sputtered at P_{tot} = 30 mTorr show 4 distinct emission peaks. Notably, the PL positions 3 and 6 in the more stoichiometric film (P_{tot} = 30 mTorr) do not show distinct peaks. However, it cannot be excluded that they are contributing to the background intensity in these regions.

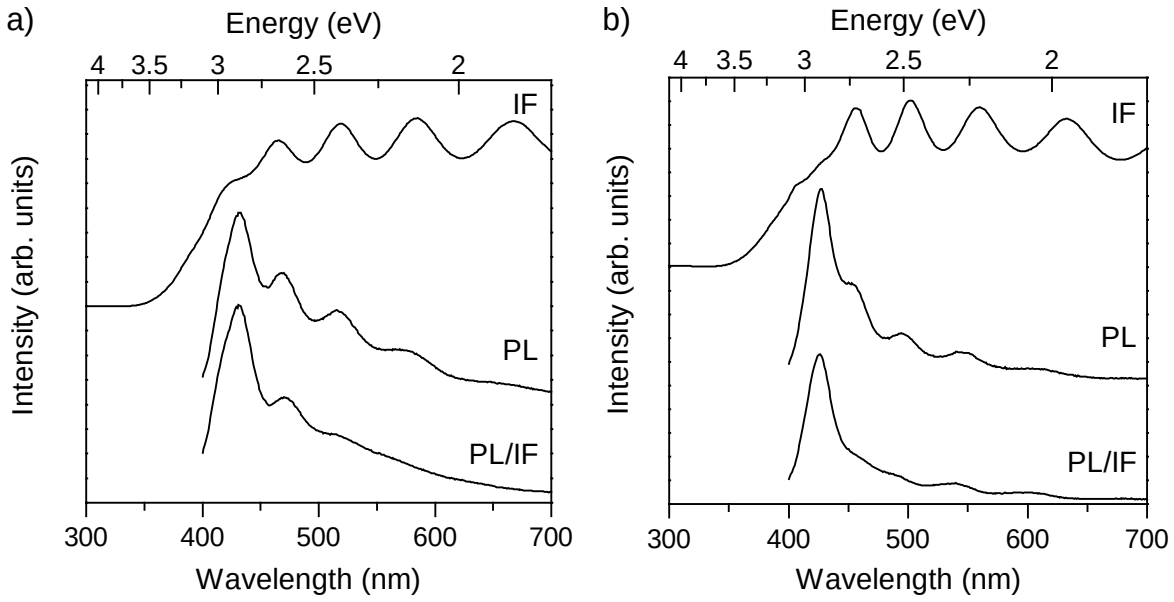

Figure 4 PL, IF and PL/IF spectra at an excitation wavelength λ = 380 nm for WO_3 films prepared with different P_{tot}: a) 30 mTorr, and b) 10 mTorr. Spectra have been shifted for clarity.

The main PL emission bands (peak 2), which are due to recombination of the photo-excited electrons at the conduction band minimum are located at 433 nm (2.86 eV) and 425 nm (2.91 eV) for the WO_3 film prepared at P_{tot} = 30 mTorr and 10 mTorr, respectively, and thus indicates an optical band gap E_g = 2.91 eV and 2.86 eV for these films. These values are in good agreement with the corresponding value of the demarcation energy, namely 440 nm (2.82 eV) obtained from the absorption coefficient α shown in Fig. 1b. At P_{tot} = 10 mTorr the WO_3 film shows a pronounced emission peak 5 at 537 nm (2.31 eV), which at P_{tot} = 30 mTorr film appears at 2.36 eV with a slightly lower relative intensity. Peak 6 at 2.07 eV is clearly observed only in the films deposited at P_{tot} = 10 mTorr . The PL emission at 2.31 eV is very close to the calculated energies of the optical levels for the ($V_o^0 \rightarrow (V_o^{1+})^*$) and ($V_o^0 \rightarrow (V_o^{2+})^*$ transitions reported by Wang et al,[17] from calculations using the B3LYP functional. Analogously, we may tentatively attribute peak 6 located at 2.07 eV with the $V_o^{1+} \rightarrow (V_o^{2+})^*$ optical transition, which is predicted at 2.11 eV by Wang et al.[17] . All these transitions take place from a relaxed initial state to an unrelaxed (denoted by *) vacancy configuration, where the electron recombines with a hole in the valence band.

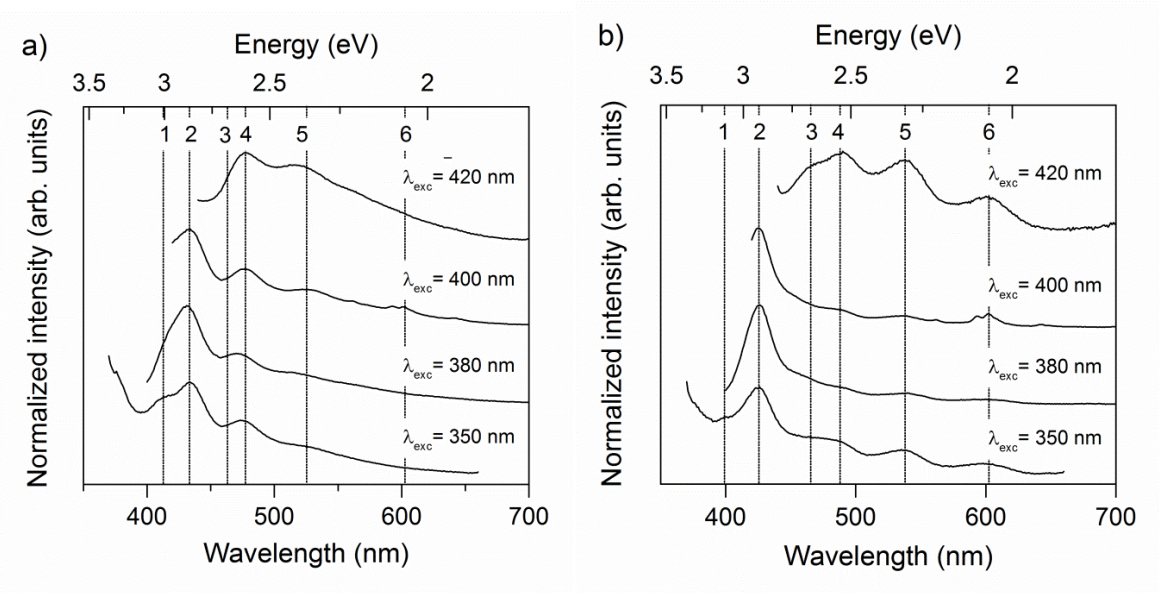

Figure 5 PL spectra at different excitation wavelengths for WO_3 films prepared with different P_{tot}: a) 30 mTorr, and b) 10 mTorr. The PL spectra have been corrected for interference by dividing them with the IF function (see text). Spectra have been shifted along the y-axis for clarity and normalized with the maxium peak intensity (peak 2 for 350, 380 and 400 nm excitation energy, and peak 4 for 420 nm excitation energy).

Table 1 Photoluminescence emission energies, relative intensities, and assignment for sub-stoichiometric (P_{tot} = 10 mTorr), and close to stoichiometric (P_{tot} = 30 mTorr) WO_3 thin films.

Peak no.	P_{tot} = 10 mTorr		P_{tot} = 30 mTorr		Type of transition§	Calculated transition levels
	(eV)	intensity ratio¤	(eV)	intensity ratio†		(eV) [Wang]
1	3.10	0.15	3.02	0.27	direct band gap	
2	2.91	1	2.86	1	band to band recombination	
3	~2.68	0.12	-	-	$(V_o^{1+})^* \rightarrow V_o^{2+} + e_{VB}$	
4	2.53	0.15	2.60	0.38	$(V_o^{0})^* \rightarrow V_o^{1+} + e_{VB}$	
5	2.31	0.13	~2.36	0.34	$V_o^{0} \rightarrow (V_o^{1+})^* + e_{VB}$	2.37
6	2.07	0.09	-	-	$V_o^{1+} \rightarrow (V_o^{2+})^* + e_{VB}$	2.11

§)"*" denotes non-relaxed states

†) The intensity ratio was calculated from the maximum peak intensity in the PL spectra at an excitation wavelength λ_{ex} = 380 nm (peak 2).

We note, however, that direct comparisons between experiments and density functional calculations, which critically depend on the position of the calculated valence and conduction bands, should be taken with caution. Nevertheless, in the work by Wang et al,[17] the hybrid functionals employed resulted in E_g values in the range of our measured ones.

The interpretation of peaks 3 and 4 is more uncertain. Both films exhibit a pronounced peak 4 at 2.53 eV (P_{tot} = 10 mTorr) and 2.60 eV (P_{tot} = 10 mTorr), and these energies are higher than those of the calculated optical transitions between V_o levels. The high relative intensity of peak 4 on the more sub-stoichiometric film prepared at P_{tot} = 10 mTorr qualitatively support that peak 4 is associated with the defect concentration. In addition, the film prepared at P_{tot} = 10 mTorr exhibits a weak shoulder (peak 3) at 465 nm (2.68 eV), which is not evident at P_{tot} = 30 mTorr. As noted by Gallino et al.,[15] a number of PL mechanisms can be significant. For example, an electron excited into the conduction band can decay non-radiatively into a V_o^{1+} state hence forming a V_o center. If the latter state does not have sufficient time to relax, the PL transition will take place in the unrelaxed $(V_o^0)^*$ configuration. This $(V_o^0)^* \rightarrow V_o^{1+}$ transition would occur at an energy larger than the associated optical transitions discussed above, and we tentatively ascribe peak 4 to this effect. Analogously, we may assume that peak 3 is due to a similar mechanism involving doubly charged vacancies, e.g. $(V_o^{1+})^* \rightarrow V_o^{2+}$. However, it should be noted that PL transitions might take place also from W^{5+} states to the valence band.

An interesting observation concerns the emission peak 1 located at 3.10 eV and 3.02 eV for the films prepared at P_{tot} = 10 mTorr and 30 mTorr, respectively. The relative intensity of this emission peak is larger for the less sub-stoichiometric WO_3 film. It is close to the direct band gap value reported for WO_3.[23] This suggests that we must distinguish between the direct band gap determined in previous reports, and the demarcation energy determined from Fig. 1. However, further studies are needed to elucidate the nature of the states at the conduction band edge (approximately 2.8 to 3.1 eV above the valence band edge).

IV. CONCLUSION

The optical properties of WO_3 thin films prepared by DC magnetron sputtering with varying degree of sub-stoichiometry, as controlled by the sputtering pressure, P_{tot}, have been measured with spectrophotometry in the 300 – 2500 nm wavelength region, and with photoluminescence (PL) spectroscopy. An optical band gap of about 2.8 eV was inferred from spectrophotometry and in PL measurements the band gap was found to be 2.91 eV and 2.86 eV for 10 and 30 mTorr WO_3 thin films, respectively. Two absorption bands were observed in the NIR region, which were correlated with oxygen vacancies. The low energy NIR peak was shown to agree well both with previously reported data for polaron absorption due to $W^{5+} \rightarrow W^{6+}$ electronic transitions between neighboring W atoms and with data for the $V_o^0 \rightarrow W^{6+}$ optical transition obtained from recent hybrid DFT calculations. The origin of the second peak, which shifts upwards in energy as a function of P_{tot}, was tentatively attributed to optical transitions involving doubly charged (V_o^{2+}) final states, with possible contribution from bipolaronic transitions. The measured PL spectra agree well with calculated optical transition energies from states localized at oxygen vacancy sites, with dominant contributions involving neutral

(V_o^{0}) and singly (V_o^{1+}) charged vacancies in the less sub-stoichiometric films, and additional contributions involving also doubly charged (V_o^{2+}) vacancy sites in the more sub-stoichiometric films. The results presented here provide new insight into oxygen vacancy induced band gap states in WO_3, and show that even slight sub-stoichiometry ($x \approx 0.001$-0.005) results in significant changes of the optical properties.

ACKNOWLWDGEMENTS

This work was partly funded by the Swedish Research Council (Grants No. VR-2010-3514 and VR-2011-3940).

References

1 G. A. Niklasson and C. G. Granqvist, J. Mater. Chem **17**, 127 (2007).
2 C. G. Granqvist, A. Azens, P. Heszler, L. B. Kish, and L. Österlund, Solar Energy Mater. Solar Cells **91**, 355 (2007).
3 P. M. Woodward, A. W. Sleight, and T. Vogt, J. Phys. Chem. Solids **56**, 1305 (1995).
4 P. M. Woodward, A. W. Sleight, and T. Vogt, J. Solid State Chem. **131**, 9 (1997).
5 N. S. Hush, Progr. Inorg. Chem. **8**, 391 (1967).
6 B. W. Faughnan, R. S. Crandall, and P. M. Heyman, RCA Review **36** (1975).
7 W. Jones and N. H. March, *Theoretical Solid State Physics* (Dover Publications, 1985).
8 I. G. Austin and N. F. Mott, Adv. Phys. **18**, 41 (1969).
9 T. He, Phys. Rev. B **51**, 16689 (1995).
10 V. V. Bryskin, Sov. Phys. Solid State **24**, 627 (1982).
11 E. Salje, Opt. Commun. **24**, 231 (1978).
12 O. F. Schirmer, V. Wittwer, G. Baur, and G. Brandt, J. Electrochem. Soc. **124**, 749 (1977).
13 A. L. Larsson, B. O. Sernelius, and G. A. Niklasson, Solid State Ionics **165**, 35 (2003).
14 E. Iguchi and H. Miyagi, J. Phys. Cem. Solids **54**, 403 (1993).
15 F. Wang, C. Di Valentin, and G. Pacchioni, J. Phys. Chem. C **115**, 8345 (2011).
16 F. Gallino, G. Pacchioni, and C. Di Valentin, J. Chem. Phys. **133**, 144512 (2010).
17 F. Wang, C. Di Valentin, and G. Pacchioni, Physical Review B **84**, 073103 (2011).
18 S. K. Deb, Sol. Energy Mater. Sol. Cells **92**, 245 (2008).
19 J. Y. Luo, F. L. Zhao, L. Gong, H. J. Chen, J. Zhou, Z. L. Li, S. Z. Deng, and N. S. Xu, Appl. Phys. Lett. **91**, 093124 (2007).
20 M. Feng, A. L. Pan, H. R. Zhang, Z. A. Li, F. Liu, H. W. Liu, D. X. Shi, B. S. Zou, and H. J. Gao, Appl. Phys. Lett. **86** (2005).
21 M. Manfredi, C. Paracchini, G. C. Salviati, and G. Schianchi, Thin Solid Films **79**, 161 (1981).
22 I. M. Szilágyi, et al., J. Catalysis **294**, 119 (2012).
23 M. B. Johansson, G. Baldissera, I. Valyukh, C. Persson, H. Arwin, G. A. Niklasson, and L. Österlund, J. Phys.: Condens. Matter **25**, 205502 (2013).
24 M. B. Johansson, G. A. Niklasson, and L. Österlund, J. Mater. Res. **27**, 3130 (2012).
25 M. B. Johansson, A. Mattsson, S.-E. Lindquist, G. A. Niklasson, and L. Österlund.
26 W. Q. Hong, J. Phys. D:Appl. Phys. **22**, 1384 (1989).
27 R. Swanepoel, J. Phys. E: Sci Instrum. **16**, 1214 (1983).
28 M. Thiess, Dr.-Bernhard- Klein-Str. 110, D-52078 Aachen, 2002).
29 L. Siozade, J. Leymarie, P. Disseix, A. Vasson, M. Mihailovic, N. Grandjean, M. Leroux, and J. Massies, Solid State Commun. **115**, 575 (2000).
30 E. K. H. Salje, Eur. J. Solid State Inorg. Chem. **31**, 805 (1994).

[31] A. S. Ferlauto, G. M. Ferreira, J. M. Pearce, C. R. Wronski, and R. W. Collins, J. Appl. Phys **92**, 2424 (2002).
[32] F. Urbach, Phys. Rev. **92**, 1324 (1953).
[33] F. Wang, C. Di Valentin, and G. Pacchioni, J. Phys. Chem. C **16**, 8345 (2011).
[34] R. Chatten, A. V. Chadwick, A. Rougier, and P. J. D. Lindan, J.Phys. Chem.B. **109**, 3146 (2005).
[35] O. F. Schirmer and E. Salje, Solid State Commun. **33**, 333 (1980).
[36] O. F. Schirmer and E. Salje, J. Phys. C: Solid State. Phys. **13**, L1067 (1980).